EDGEWOOD
RESEARCH, DEVELOPMENT & ENGINEERING CENTER
U.S. ARMY CHEMICAL AND BIOLOGICAL DEFENSE COMMAND

ERDEC-TR-467

RANDOM VIBRATION ANALYSIS OF THE XM21 DECONTAMINANT PUMPER MODULE OF THE MODULAR DECONTAMINATION SYSTEM

Stephen J. Colclough

ENGINEERING DIRECTORATE

February 1998

Aberdeen Proving Ground, MD 21010-5423

Disclaimer

The findings in this report are not to be construed as an official Department of the Army position unless so designated by other authorizing documents.

REPORT DOCUMENTATION PAGE

Form Approved
OMB No. 0704-0188

1. AGENCY USE ONLY (Leave Blank)	2. REPORT DATE	3. REPORT TYPE AND DATES COVERED
	1998 February	Final; 97 Jan - 97 Jun

4. TITLE AND SUBTITLE

Random Vibration Analysis of the XM21 Decontaminant Pumper Module of the Modular Decontamination System

5. FUNDING NUMBERS

PR-643884DDE4

6. AUTHOR(S)

Colclough, Stephen J.

7. PERFORMING ORGANIZATION NAME(S) AND ADDRESS(ES)

DIR, ERDEC, ATTN: SCBRD-ENE-E, APG, MD 21010-5423

8. PERFORMING ORGANIZATION REPORT NUMBER

ERDEC-TR-467

9. SPONSORING/MONITORING AGENCY NAME(S) AND ADDRESS(ES)

10. SPONSORING/MONITORING AGENCY REPORT NUMBER

11. SUPPLEMENTARY NOTES

12a. DISTRIBUTION/AVAILABILITY STATEMENT

Approved for public release; distribution is unlimited.

12b. DISTRIBUTION CODE

13. ABSTRACT (Maximum 200 words)

The XM21 Decontaminant Pumper module of the Modular Decontamination System was analyzed using finite element analysis techniques to show why the first design iteration passed transportation vibration testing, the current design iteration did not, and whether the proposed changes to the system will pass. The baseplate in the current design developed a fatigue crack at a weld when vibration tested. The failure was caused by the switching of position between the pump and the alternator. This was the only change between the two systems. The results of the analyses show that switching the pump from the right side to the left side causes a 28% increase in the stress level of the weld that failed from 9,758 to 12,495 psi. A modification to the pump/alternator support bracket was proposed as a solution to the failure, and this design was also analyzed. The proposed design analysis results showed that the weld stress levels were improved to be 22% lower than the first design and 39% lower than the current design. The stress in the weld that failed was reduced to 6,834 psi. The proposed design change will eliminate the failure experienced in the current design.

14. SUBJECT TERMS

XM21	Random vibration
Decontaminant pumper	Finite element analysis
Modular decontaminant system	Power spectral density analysis

15. NUMBER OF PAGES

27

16. PRICE CODE

17. SECURITY CLASSIFICATION OF REPORT	18. SECURITY CLASSIFICATION OF THIS PAGE	19. SECURITY CLASSIFICATION OF ABSTRACT	20. LIMITATION OF ABSTRACT
UNCLASSIFIED	UNCLASSIFIED	UNCLASSIFIED	UL

NSN 7540-01-280-5500

Standard Form 298 (Rev. 2-89)
Prescribed by ANSI Std. Z39-18
298-102

Blank

PREFACE

The work described in this report was authorized under Project No. 643884DDE4, Decontamination. This work was started in January 1997 and completed in June 1997.

The use of either trade or manufacturers' names in this report does not constitute an official endorsement of any commercial products. This report may not be cited for purposes of advertisement.

This report has been approved for public release. Registered users should request additional copies from the Defense Technical Information Center; unregistered users should direct such requests to the National Technical Information Service.

Blank

CONTENTS

1. Introduction 7

2. Finite Element Model 7

3. Fatigue Endurance Limit 14

4. Analysis and Results 16

5. Discussion 20

6. Conclusions 22

References 23

APPENDIXES

A. Power Spectral Density (PSD) Values 25

B. Individual System Natural Frequencies 27

FIGURES

1 XM21 Decontaminant Pumper Unit 8
2 XM21 DP Baseplate 9
3 XM21 Baseplate Fatigue Fracture 9
4 XM21 DP on Vibration Table 10
5 Finite Element Model with Constraints 11
6 Finite Element Model Three View 12
7 Baseplate Shell Element Plot 13
8 Illustration of Three Design Configurations 14
9 Element Plot of Joint Solid Model 15
10 Frame Bending Moments for Old Design (lb-in) 17
11 Frame Bending Moments for Current Design (lb-in) 18
12 Frame Bending Moments for Proposed Design (lb-in) 19
13 Von Mises Stress in Solid Model of Weld 21

TABLES

1 Von Mises Equivalent Stresses in Weld Joints 20
2 Corrected Von Mises Equivalent Stresses in Weld Joints 20

RANDOM VIBRATION ANALYSIS OF THE XM21 DECONTAMINANT PUMPER MODULE OF THE MODULAR DECONTAMINATION SYSTEM

1. Introduction

The XM21 Decontaminant Pumper (DP) module of the Modular Decontamination System (MDS) is a field transportable system developed for applying and scrubbing liquid decontaminants (Figure 1). The XM21 consists of a tubular aluminum frame, a shock mounted aluminum angle baseplate weldment, an aluminum pump/alternator support bracket, a diaphragm pump, an alternator, and a 325 cubic centimeter displacement diesel engine.

The XM21 DP is transported around the battlefield in a two–wheel trailer which subjects it to numerous random vibrations. To qualify the structural integrity of system designs without physically hauling each design iteration around full scale transportation test courses, a Power Spectral Density (PSD) vibration simulation was developed. The PSD excitation was measured in g^2/Hz. The PSD simulation values are given in Appendix A.

The XM21 DP had successfully passed the transportation vibration tests when a design change was adopted to swap the location of the pump and alternator. This change required that the transportation tests be repeated to re–qualify the system. This change was not expected to cause any problems so six XM21 systems were ordered of this design to be used in additional testing. When this latest design iteration was subjected to the transportation vibration simulation on a vibration machine, a fatigue failure occurred in the baseplate weldment (Figures 2 and 3). This failure halted testing and necessitated another redesign of the XM21 DP.

The purpose of the analysis presented here is to show the stress level differences between the design iteration that passed the transportation simulation, the iteration that failed, and the proposed solution to the failure using finite element analysis PSD techniques.

2. Finite Element Model

A three dimensional finite element model was created to simulate the condition of the XM21 DP when tested on a vibration table. The XM21 DP as it appeared on the vibration table is shown in Figure 4. The finite element model consisted of several different element types. BEAM4, three dimensional beam elements were used to model all the tubular frame members and all massless and rigid connecting members. BEAM44, three dimensional unsymmetric beam elements were used to model the U–channel members supporting the baseplate and 90° angle control panel support members. SHELL63, three dimensional plate elements were used to model the baseplate and frame stiffening gussets. LINK8, three dimensional spar elements were used to model the tie–down straps and MASS 21, structural mass elements were used to model the engine, pump, alternator, and alternator/pump support bracket. Figures 5, 6, and 7 show the finite element model.

The level of detail in the model was reduced to allow more efficient use of computing resources and modeling time while still providing required results. All bolts, welds, and fillets were eliminated. The pump, alternator, engine, and pump/alternator support bracket

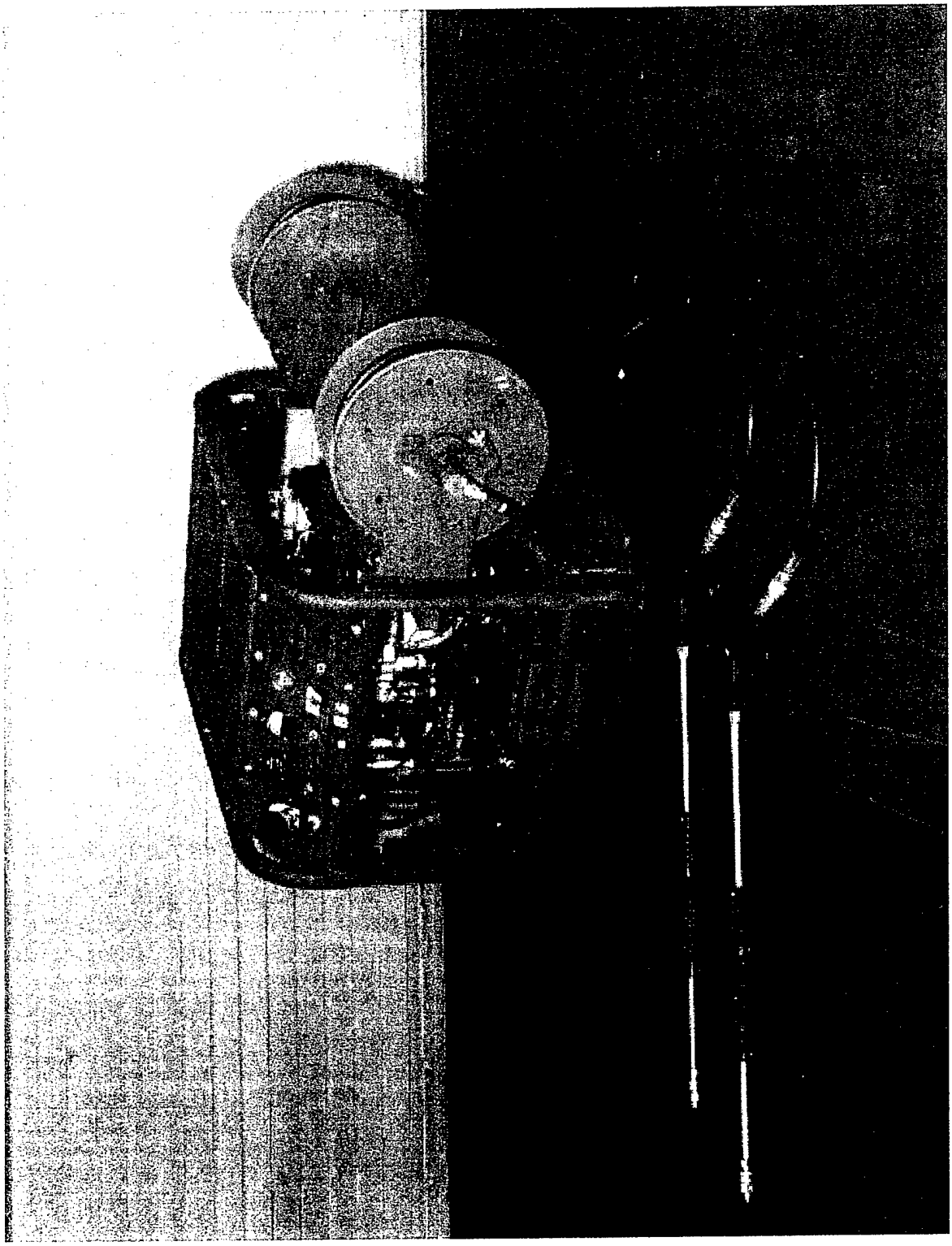

Figure 1: XM21 Decontaminant Pumper Unit

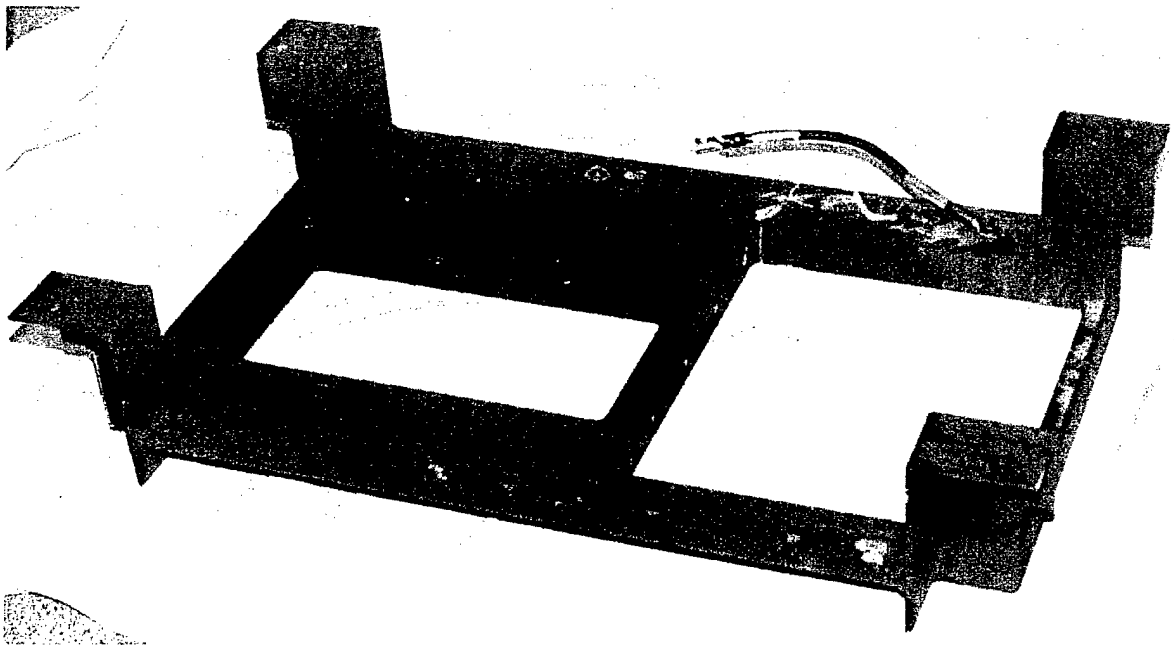

Figure 2: XM21 DP Baseplate

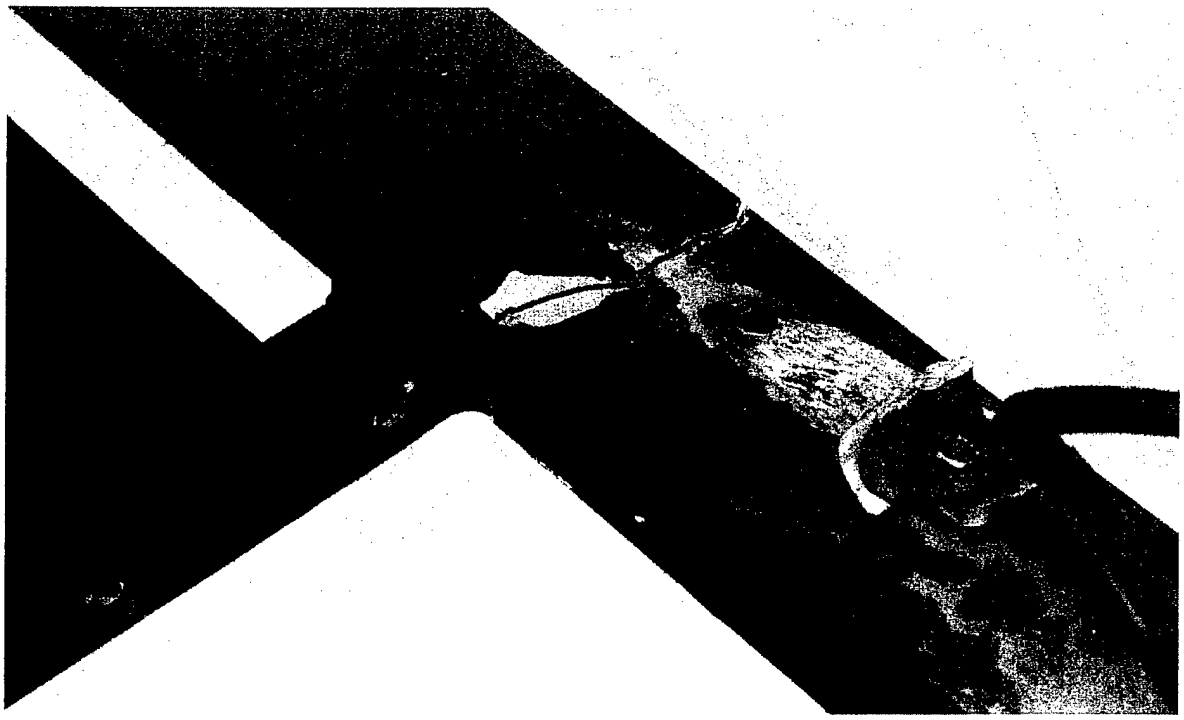

Figure 3: XM21 Baseplate Fatigue Fracture

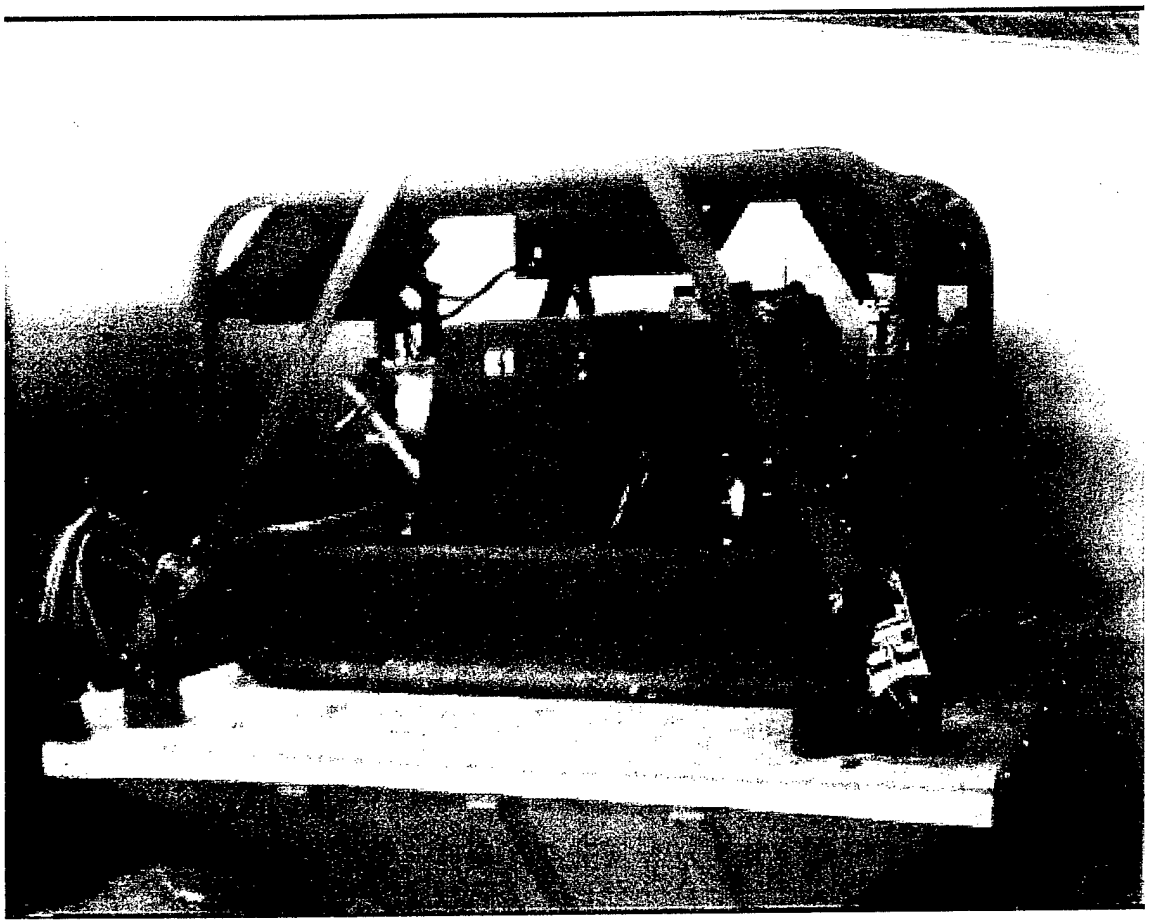

Figure 4: XM21 DP on Vibration Table.

were modeled as point masses and rigidly connected to their respective bolt down locations on the baseplate.

The frame tube and U–channel material was 6061–T6 aluminum with a Young's Modulus of 10E6 psi and a Poisson's Ratio of 0.33. The baseplate material was 5456–H111 aluminum and the tie down strap material was Nylon 6/6. The material properties of Nylon 6/6 were Young's Modulus of 471.1 ksi and Poisson's Ratio of 0.3.

Three separate models were created to analyze each of the different design iterations. The first model represented the original system configuration that had successfully passed transportation testing. The second model represented the system configuration that experienced the baseplate fatigue failure. It was the same as the first model only with the pump and alternator switching positions about the centerline of the system. The third model represented the proposed solution to the failure (Figure 8). This model had the same component configuration as the second model except that the alternator/pump support

Figure 5: Finite Element Model with Constraints

Figure 6: Finite Element Model Three View

Figure 7: Baseplate Shell Element Plot

bracket was modified to incorporate the increased side plate length on the side of the system where the failure occurred.

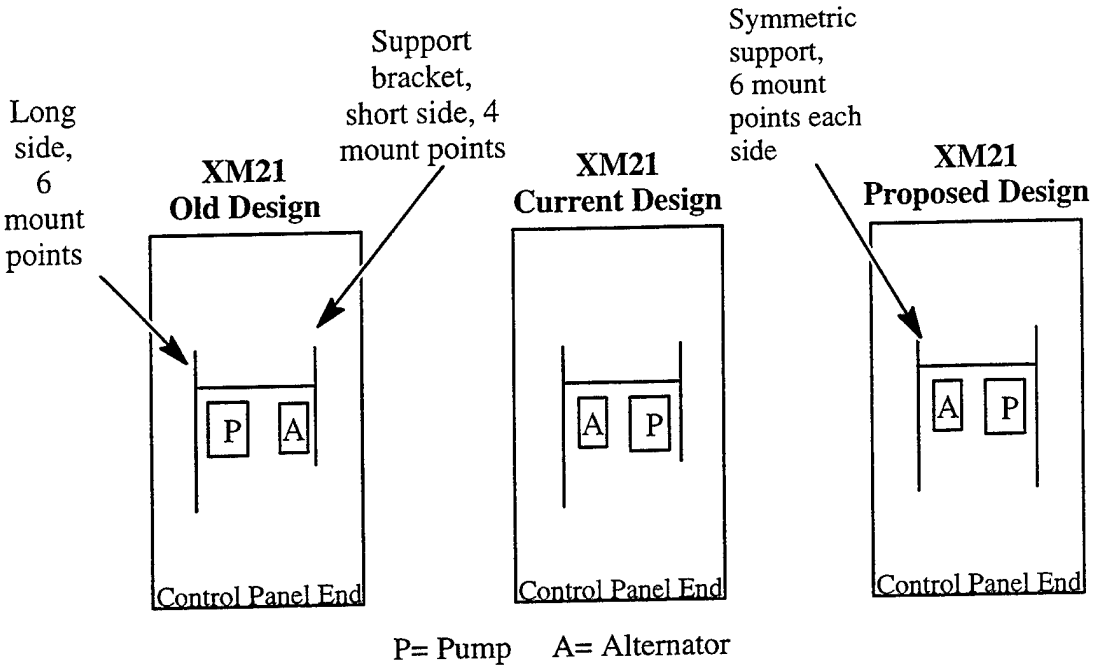

Figure 8: Illustration of Three Design Configurations

An additional solid element model was created of the joint that failed (Figure 9). This solid model included the actual geometry of the joint including weld fillets. The purpose of this model was to examine how the stresses developed at the vicinity of failure in order to develop a reasonable stress concentration factor. This stress concentration factor was applied to the shell element stress results to show values of reasonable magnitude. The loading of this model consisted of constraining the representative longitudinal member and applying a 100 psi load to the end face of the cross–member. The 100 psi load value was used to allow the maximum stress in the weld to be divided by this load value to get the stress concentration factor.

3. Fatigue Endurance Limit

The fatigue endurance limit needs to be calculated to determine if the stress in the weld joints is high enough to limit the amount of stress cycles the joints can see. The endurance limit for a material is the highest level of alternating stress that can be withstood indefinitely without failure [1,2].

Aluminum 5456–H111 did not have a listed endurance limit, so the yield strength (33,000 psi) was used as the endurance limit. The endurance limit for a material (S_n) is

Figure 9: Element Plot of Joint Solid Model

determined by testing precision machined, highly polished specimens. This endurance limit needs to be corrected (S_n') for actual use conditions such as stress concentrations(K_f), surface finish(C_S), size (C_G), and other factors.

$$S_n' = \frac{S_n C_G C_S}{K_f} \qquad (1)$$

In determining the corrected endurance limit (S_n'), Equation 1, for the material in the weld joints, three correction factors were applied. The first correction factor applied was a stress concentration for the T–butt joint weld of K_f=2.0. The second correction factor used was for surface finish. A correction factor of C_S=0.7 was used to account for the surface condition due to welding. The final correction factor used was a size factor C_G=0.8. This factor is used to account for the stress gradient between the most extreme material and the neutral axis of the member (Juvinall and Marshek, 1991, p. 270 and 420).

The corrected endurance limit for aluminum 5456–H111 used in the baseplate was calculate to be 9,250 psi.

4. Analysis and Results

A separate analysis was run for each design iteration model. The complete PSD random vibration analysis required two steps. The first step was to run a modal analysis to determine all the system natural frequencies, or modes, between 5 Hz and 500 Hz. The Block Lancoz method was used to extract the modes of the system. The second step was to run a spectrum PSD analysis using the spectrum data for the vertical, transverse, and longitudinal directions. The spectrum analysis used the system natural frequencies from step one.

The modal analysis for each of the designs calculated forty different natural frequencies, or modes, for each of the systems between 5 Hz and 500Hz.. The first natural frequency occurred between 36 Hz and 40 Hz for all three systems. The second natural frequency occurred between 49 Hz and 56 Hz for all three systems. The third natural frequency for each system occurred at 68 Hz. The remaining natural frequencies for each system can be found in Appendix B.

The PSD spectrum analysis used the PSD data from Appendix A to calculate the 1–σ values for displacement, stress, and member forces for each system. The results are for all three PSD spectrums acting simultaneously. The 1–σ values represent the maximum displacement, stress, and member forces that the system will see 68% of the time.

The XM21 DP baseplate was symmetric about its longitudinal axis. This meant that there was another weld identical to the one that failed. This provided a control weld for results comparison with the failed weld joint.

The 1–σ bending moments for the tubular frame members for each design iteration are shown in Figures 10, 11, and 12. The maximum bending moment in the frame for the

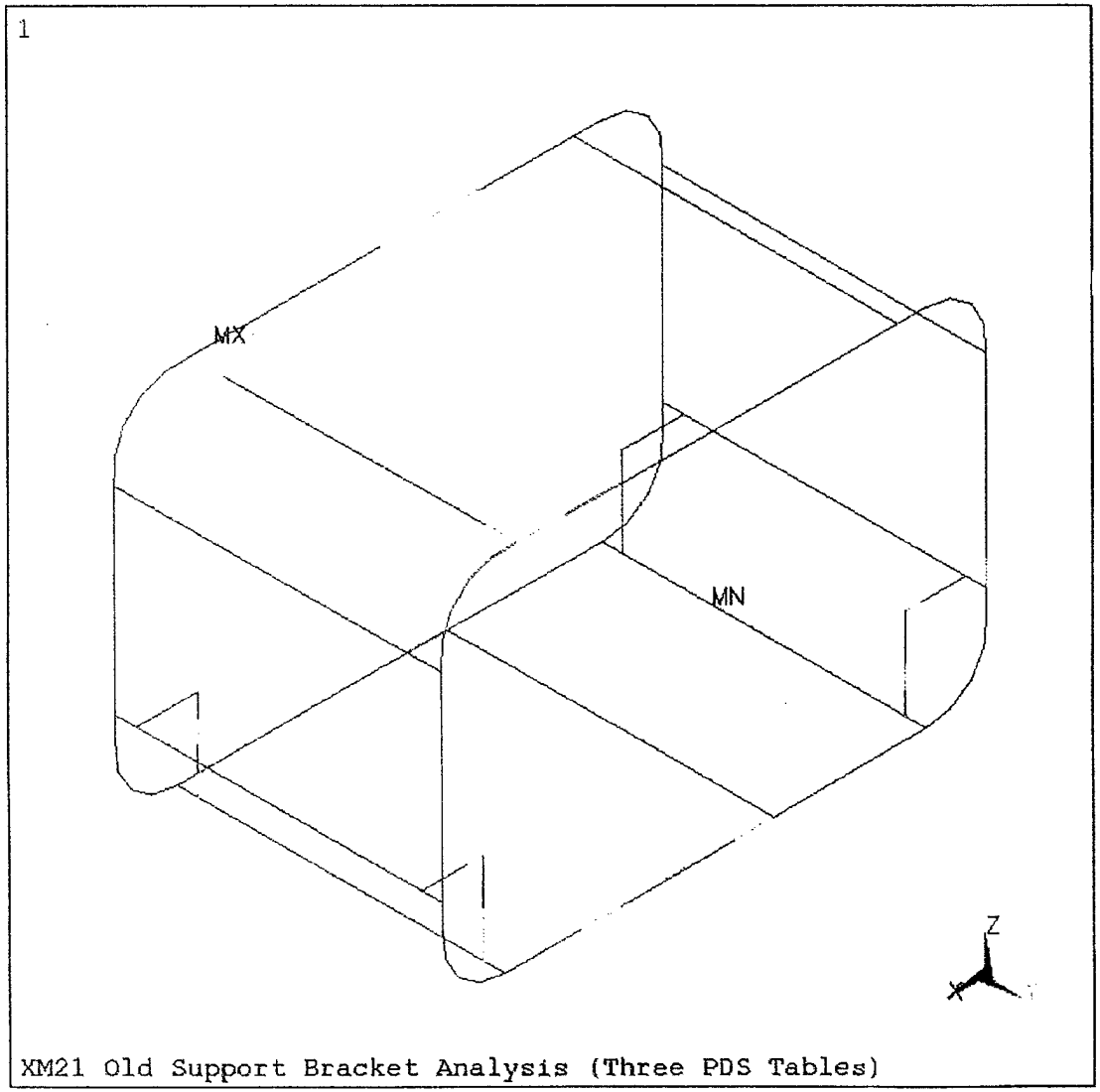

Figure 10: Frame Bending Moments for Old Design (lb–in).

Figure 11: Frame Bending Moments for Current Design (lb–in).

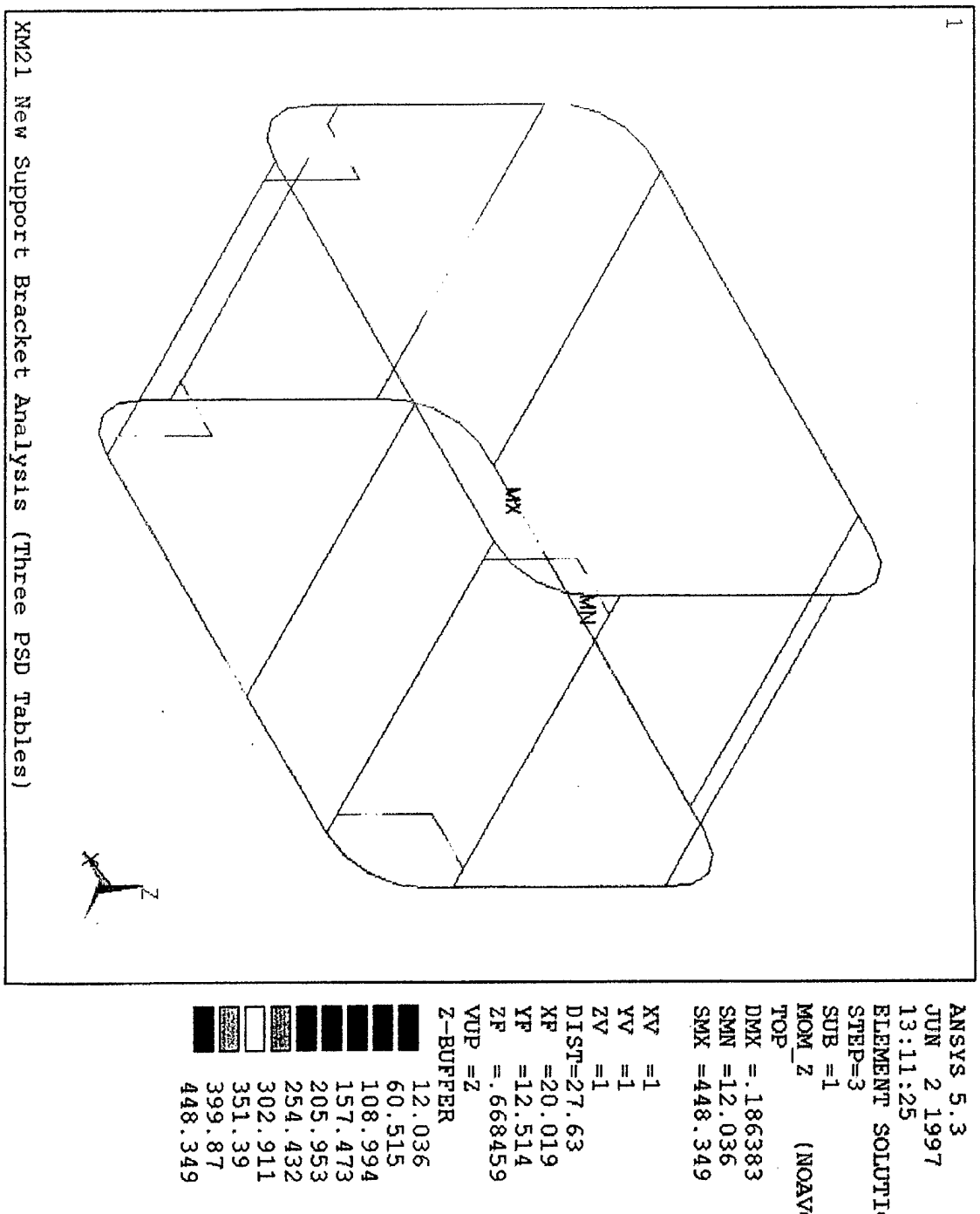

Figure 12: Frame Bending Moments for Proposed Design (lb–in).

original design configuration was 668 lb–in. The maximum bending moments in the current and proposed design configurations were 611 lb–in and 448 lb–in, respectively.

The 1–σ results generated by the analysis software for the failed weld and its symmetrical counterpart are presented in Table 1. The values presented in the table are Von Mises Equivalent stresses and were acquired with all shell elements in the baseplate selected. These values represent the stress at the outside corner along the bottom of the cross–member beam. The right and left side of the XM21 DP are defined by facing the system from the end with the control panel.

Table 1: Von Mises Equivalent Stresses in Weld Joints.

	Old Design (psi)	Current Design (psi)	Proposed Design (psi)
Right Side Weld	508	439	445
Left Side Weld	574	735	402

The stress levels in Table 1 were not of a meaningful magnitude to make any determinations other than relative changes between the three different designs. Since the baseplate model in the PSD analysis did not include the effects of weld fillets, a solid model of only the joint geometry was analyzed. This analysis showed a stress concentration in the area of the weld fillet where the failure occurred in the baseplate (Figure 13). The equivalent stress plot , Figure 13, shows that the stress in the weld is approximately seventeen times higher than the stress in the remainder of the cross–member. A factor of seventeen was adopted as a stress concentration factor for this particular weld joint geometry. Table 2 shows the weld joint stresses with the stress concentration factor applied.

Table 2: Corrected Von Mises Equivalent Stresses in Weld Joints.

	Old Design Corrected (psi)	Current Design Corrected (psi)	Proposed Design Corrected (psi)
Right Side Weld	8,636	7,463	7,565
Left Side Weld	9,758	12,495	6,834

5. Discussion

The 1–σ results show that the proposed design change to the XM21 DP would work as intended in increasing the system's transportation survivability. The stress levels in the weld joints are above the corrected endurance limit , so the baseplate could fail in the left

Figure 13: Von Mises Stress in Solid Model of Weld

side weld joint if enough stress cycles are realized. Comparing the results between the old design and the current design shows a 28 percent increase of stress in the welds being examined. In the old design, with the pump on the left side, the weld joint on the left side had the highest stress (9,758 psi) of the two weld joints. This stress level was proven to be low enough not to cause fatigue failure by successfully passing the vibration test. In the current design, with the pump on the right side, the weld joint on the right side now has the highest stress (12,495 psi)of the two weld joints. This 28 percent increase in the stress level of the weld joints was high enough to trigger a fatigue failure in vibration testing.

The results from the proposed design show reduction in weld stresses compared to the two previous designs. The proposed design shows a 39 percent stress reduction when compared to the highest weld stress in the current design and a 22 percent reduction when compared to the highest weld stress in the old design.

The maximum bending moment in the frame members comparing all three designs was 668 lb–in. This corresponds to a bending stress of 2,947 psi and occurred in the old system design. The new system design has a maximum bending stress of 1,976 psi in any of the frame members.

6. Conclusions

1. The proposed design change for the alternator/pump support bracket will reduce the stress in the area of the baseplate weld failure in the current design.
2. The proposed design change does not cause any increased stresses in frame members and actually reduces them.
3. The proposed new design should experience no structural problems in random vibration testing due to the stresses in the new design being lower than the old design, which had successfully passed this testing.

References

1. ANSYS Revision 5.3 software, ANSYS Inc., Canonsburg, PA, 1996.

2. Juvinall, R.C., Marshek, K.M., Fundamentals of Machine Component Design, pp 257–295, 410–420, John Wiley & Sons, New York, NY, 1991.

3. Shigley, J.E., Mitchell, L.D., Mechanical Engineering Design, 4th ed., pp 270–342, McGraw–Hill, New York, NY, 1983.

Blank

Appendix A

Power Spectral Density (PSD) Values

Lateral Direction (Y–Axis)		Longitudinal Direction (X–Axis)		Vertical Direction (Z–Axis)	
Hz	G^2/Hz	Hz	G^2/Hz	Hz	G^2/Hz
5.000	.006140	5.000	.003530	5.000	.038680
6.666	.004840	5.833	.002580	5.833	.033370
10.830	.001660	6.666	.004310	6.666	.033890
12.500	.001240	7.500	.019400	7.500	.180100
15.000	.001620	8.333	.011960	8.333	.155300
15.830	.006510	10.000	.057560	10.830	.005990
16.660	.008250	10.830	.004710	15.000	.001730
17.500	.002600	12.500	.002260	16.660	.007370
20.000	.002110	13.330	.001980	18.330	.002940
22.500	.001660	15.000	.003300	20.830	.005820
28.330	.001070	15.830	.010950	22.500	.003960
33.330	.009570	16.660	.015960	25.000	.012940
35.000	.004300	17.500	.007340	27.500	.005990
40.000	.002930	20.000	.008030	28.330	.003840
42.500	.007780	20.830	.004820	31.660	.007600
43.330	.003110	22.500	.006020	33.330	.007160
46.660	.002680	25.000	.040540	38.330	.001140
50.000	.008250	30.000	.002760	40.000	.001210
56.660	.006320	30.830	.004930	42.500	.008060
60.000	.004430	32.500	.010710	45.830	.003220
62.500	.000847	36.660	.002580	50.000	.011500
166.600	.001360	40.000	.005150	62.500	.003620
176.600	.000750	41.660	.007850	68.330	.007600
187.500	.001070	45.830	.004040	90.000	.002120
213.300	.004040	47.500	.007180	95.000	.005170
242.500	.001070	96.670	.001890	128.300	.000980
338.300	.000252	123.300	.001700	150.800	.002690
500.000	.000060	138.300	.001040	171.600	.001490
		146.600	.001650	180.000	.002940
		176.600	.004610	195.800	.005020
		190.000	.006390	210.800	.001140
		213.300	.000430	225.800	.002940
		293.300	.000950	253.300	.005490
		396.600	.000560	265.000	.003420
		485.800	.000160	288.300	.001170
		500.000	.000160	338.300	.000710
				363.000	.002320
				485.800	.000110
				500.000	.000110

Blank

Appendix B

Individual System Natural Frequencies

B: System Natural Frequencies

Number	Old Design (Hz)	Current Design (Hz)	Proposed Design (Hz)
1	36.16	37.80	39.23
2	49.11	52.16	56.28
3	68.02	68.05	68.07
4	74.42	74.43	74.46
5	93.37	93.40	93.45
6	113.17	113.18	113.18
7	115.32	115.33	115.37
8	123.22	125.18	125.21
9	125.24	127.90	133.36
10	156.65	150.24	154.66
11	190.96	191.05	191.30
12	212.72	213.42	214.60
13	221.37	221.85	223.33
14	233.47	233.64	239.93
15	242.57	243.23	247.00
16	256.33	253.16	257.67
17	258.28	257.80	266.95
18	265.27	268.55	269.10
19	269.20	269.21	294.65
20	289.35	295.01	333.45
21	300.88	333.13	338.22
22	335.75	343.69	351.69
23	351.73	351.74	358.85
24	361.47	362.17	362.90
25	366.12	366.28	367.36
26	380.32	379.89	380.44
27	381.00	380.38	386.66
28	393.52	394.07	394.53
29	398.14	397.48	398.26
30	418.98	419.29	419.91
31	430.06	429.98	430.01
32	438.69	438.75	439.03
33	441.82	441.85	441.90
34	449.29	449.18	449.50
35	457.01	457.80	459.33
36	467.79	470.87	472.02
37	471.97	472.31	473.45
38	484.17	489.05	491.68
39	489.72	492.39	494.15
40	494.26	494.49	499.70